Activation Mechanism of the Human Histamine H4 Receptor - An Explicit Membrane Molecular Dynamics Simulation Study

Balázs Jójárt,[#,†,‡] Róbert Kiss,[#,§,||] Béla Viskolcz,[†] and György M. Keserű*[,||,⊥]

Department of Chemistry and Chemical Informatics, Faculty of Education, University of Szeged, Boldogasszony sgt. 6., H-6725 Szeged, Hungary, Department of Pharmacodynamics and Biopharmacy, Faculty of Pharmacy, University of Szeged, Eötvös u. 6., H-6720 Szeged, Hungary, Department of Pharmaceutical Chemistry, Semmelweis University, Hõgyes Endre u. 9., H-1092 Budapest, Hungary, Gedeon Richter Plc, Gyömrõi út 19-21., H-1103 Budapest, Hungary, and Department of General and Analytical Chemistry, Budapest University of Technology and Economics, Szt. Gellért tér 4., H-1111 Budapest, Hungary

Received December 4, 2007

Molecular dynamics (MD) simulations in a membrane-embedded environment were carried out on the homology model of the human histamine H4 receptor (hH4R) alone and in complex with its endogenous activator histamine and with the first reported selective hH4R antagonist JNJ7777120. During the simulation of the histamine-hH4R complex, considerable changes occurred in the hH4R structure as well as in the interaction pattern of histamine at the binding site. These changes are in agreement with experimental data published on GPCR activation. In particular, the intracellular side of TM helix VI moved significantly away from TM helices III and VII. Moreover, histamine formed an interaction with Asn147 (4.57) that was previously proved to be important in hH4R activation. Results of the MD simulations of the native hH4R and the JNJ7777120-hH4R complex suggest that these models represent an inactive conformation of hH4R. MD simulation in the presence of JNJ7777120 resulted in the movement of the intracellular side of TM helix VI in the direction of TM helix III. Snapshots of the simulations may serve as functionally relevant models in the development of novel hH4R ligands in the future.

1. INTRODUCTION

G-protein-coupled receptors (GPCR) form one of the largest protein families in vertebrates.[1] They provide the signaling pathway for many hormones, neurotransmitters, neuromodulators, and even for odorants, flavors, and light. GPCRs are transmembrane receptors, and they share a common structural fold of seven α membrane-spanning helices and an α helix running parallel with the membrane surface. They contain conserved motifs, such as a disulfide bridge, D(E)RY sequence, and NPxxY sequence. Despite the overriding therapeutic importance of GPCRs,[2] until quite recently, bovine rhodopsin (BR) was the only GPCR with an experimentally determined 3D structure.[3] During the preparation of this manuscript, the first crystal structures of a human GPCR were reported. Kobilka and his co-workers determined the 3D structure of the human β2 adrenergic receptor (hβ2AR) in complex with Fab with a resolution of 3.4/3.7 Å.[4] The same group was able to crystallize the receptor with an exchanged third intracellular loop (IC3) in complex with the partial inverse agonist carazolol with a resolution of 2.4 Å.[5] In view of reported success stories, disclosure of these fundamental results does not fade the usefulness of the BR crystal structure serving as a reliable template for building relevant 3D models of other GPCR structures by means of homology modeling. On the contrary, the recently determined high resolution crystal of hβ2AR will facilitate GPCR homology modeling, especially in the field of aminergic receptors. The application of homology models has been proved to be useful in the interpretation of experimental data at the molecular level, e.g. by ligand docking and binding site analysis.[6–9] Recently, some authors reported the application of homology models for virtual screening.[10–13] The success of these models in structure-based drug design as well as the recently published hβ2AR crystals further supports the hypothesis that GPCRs have a similar architecture. Furthermore, it is assumed that these receptors transmit external signals in a similar fashion, i.e. they possess a common activation mechanism with individual subtleties.

At the beginning, GPCR homology models were built in vacuum, which represents a highly unrealistic environment comparing it with the physiological membrane-embedded conditions. In the past few years, however, membrane-embedded GPCR homology models were published.[14–18] In the case of these models, even molecular dynamics (MD) simulations can be carried out without any constraints, which can significantly improve the quality of the model. These simulations—especially in the presence of agonist ligands—can provide information about the activation mechanism of GPCRs. Although, the exact mechanism of GPCR activation is not fully understood, experimental data suggest the

* Corresponding author phone: +36-1-4314605; fax: +36-1-4326002; e-mail: gy.keseru@richter.hu. Corresponding author address: Department of General and Analytical Chemistry, Budapest University of Technology and Economics, Szt. Gellért tér 4., H-1111 Budapest, Hungary.
[#] These authors contributed equally to this work.
[†] Faculty of Education, University of Szeged.
[‡] Faculty of Pharmacy, University of Szeged.
[§] Semmelweis University.
[||] Gedeon Richter Plc.
[⊥] Budapest University of Technology and Economics.

10.1021/ci700450w CCC: $40.75 © 2008 American Chemical Society
Published on Web 06/23/2008

separation of the cytoplasmic ends of TM helix III (TM3) and TM helix VI (TM6) relative to each other.[19,20]

The histamine H4 receptor (H4R) is the novel member of the histamine receptor family. It belongs to the amine-binding GPCRs in subfamily "A". H4R occurs in the bone marrow, spleen, eosinophils, mast cells, basophils, CD8+ T cells, and dendritic cells.[21–25] It mediates histamine-induced chemotaxis in mast cells and eosinophils, and this effect can be blocked by selective H4 antagonists.[23,26,27] H4R shows the highest structural homology to histamine H3 receptor (H3R). Shin et al. have shown that Asp94 (3.32 − Ballesteros-Weinstein numbering)[28] and Glu182 (5.46) are crucial in both histamine binding and activation of the human H4R (hH4R).[29] In this study, the role of several other residues was also investigated. Mutating Thr178 (5.42) or Ser179 (5.43) to Ala has only a minor effect on histamine binding or hH4R activation. On the other hand, Asn147 (4.57) and Ser320 (6.52) seem to play a role in the activation process.

In our previous work,[30] we proposed a binding mode of histamine and JNJ7777120 at the hH4R binding site supported by docking calculations, surface, and binding mode analyses. In this study, we report the molecular dynamics simulation of hH4R alone and in complex with an agonist (histamine) and an antagonist (JNJ7777120) in a POPC membrane environment. On the one hand, we aimed to analyze the changes occurring during the MD simulations. On the other hand, we aimed to develop relevant hH4R models relaxed in a membrane environment that can be used in structure-based drug design of hH4R agonists and antagonists.

2. MATERIALS AND METHODS

Homology models of the hH4R alone and in complex with histamine and JNJ7777120 were developed previously (indicated as "Model B", "Model D", and "Model F", respectively, in ref 30). These models were built by using the crystal structure of BR as a template, which was the only GPCR with an experimentally determined 3D structure that time. The complex structures were obtained after docking calculations and subsequent optimization.[30] Our hH4R models contain all the extracellular (EC) and intracellular (IC) loops, except IC3, since this region comprises almost 100 residues. In contrast, this loop comprises only 25 residues in BR that prevents its application as homology modeling template. Since reliable modeling of such long, flexible loops is rather limited, we truncated this loop to the corresponding length in BR.[31] It should be noted that even the recently reported structure of hβ2AR would be a suboptimal template to model the IC3 loop of hH4R, since this flexible region was replaced to obtain diffracting crystals. Moreover, the IC3 loop of the native hβ2AR is also shorter than that of hH4R, as it contains 50−60 residues.

Histamine was considered as a monocation (protonated on the ethylamine side chain) in the N(τ) form (protonated on N(3) and deprotonated on N(1)) (Figure 1), as supported by previous Pallas calculations[30] as well as other available theoretical[32,33] and experimental data[34,35] on histamine and its derivatives.

JNJ7777120 was also considered as a monocation, protonated on the piperazine ring based on our previous Pallas calculation (Figure 1).[30]

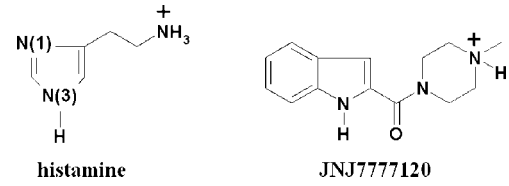

Figure 1. Structure of histamine and JNJ7777120.

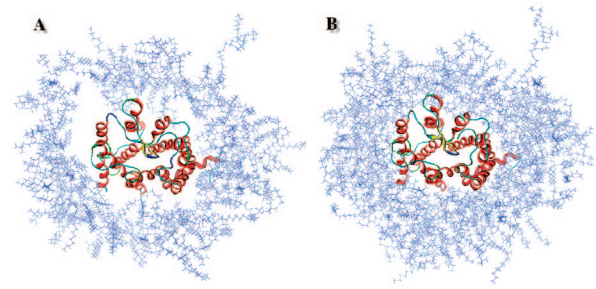

Figure 2. The native hH4R-membrane system before (A) and after (B) protein backbone restrained MD calculations. Lipids in 10 Å distance range of any protein atoms are only depicted.

A pre-equilibrated POPC/TIP3P membrane system was used for the MD simulations that was previously proved to be stable, and it reproduced the experimental data available on native membranes.[36] This POPC membrane was duplicated in *x* dimension. Then, the native hH4R (indicated as "Model B" in ref 30) was inserted manually into the membrane as the eighth helix (H8) was parallel to the *xy* plane (the membrane normal was the *z* axis). Lipids that were in close contact with the protein atoms (<0.5 Å distance from any protein atoms) were removed, and water molecules were added to the system. As a consequence of the lipid deletion, gaps were evolved between the protein and the POPC interface (Figure 2A).

Therefore, to avoid protein degradation an equilibration was performed on the native hH4R to remove these gaps using the NAMD 2.6 program package.[37] The equilibration protocol can be seen in Table 1.

This protocol yielded a more favorable membrane environment for inserting a GPCR than the initial system (Figure 2B). The resulting POPC/TIP3P system may be applied for MD simulation of other GPCRs in the future. Accordingly, the coordinates of the POPC and water molecules in the last frame of this calculation was used in the preparation of the POPC/TIP3P environment for the histamine-hH4R and the JNJ7777120-hH4R complexes ("Model D" and "Model F" in ref 30, respectively) (see Figure S1 in the Supporting Information).

The ProPka program,[38] implemented in the PDBQPR program package,[39] was utilized to assign the protonation states to the titratable groups of hH4R at the pH value of 7.4.

The charges of histamine and JNJ7777120 were calculated according to the RESP methodology.[40] Four conformations were selected from conformational sampling, utilized with the MOE 2005.06 program package.[41] These structures were optimized at the HF/6−31G* level of theory by Gaussian03.[42] The frequency calculation of the optimized ligand conformers revealed no imaginary frequencies; therefore, these structures are in true energy minimum. The molecular electrostatic potentials were calculated at the same level of

Table 1. Equilibration Protocol of the Native hH4R-POPC/TIP3P System

minimization	20000 steps with fixed protein, POPC atoms (force constant: 500 kcal/mol Å^2)
	20000 steps with fixed protein, water and chlorine atoms (force constant: 500 kcal/mol Å^2)
	20000 steps with fixed protein backbone atoms, POPC, water and chlorine atoms (force constant: 500 kcal/mol Å^2)
	10000 steps with restrained protein backbone atoms (force constant: 20 kcal/mol Å^2)
heating	from 10 to 310 K in 64 ps (NVT ensemble, $\delta t = 1$ fs, $\Delta T = 20$ K, $\Delta t = 4$ ps) with restrained protein backbone atoms (force constant: 20 kcal/mol Å^2)
equilibration MD	NPγT ensemble, $\delta t = 1$ fs, $\Delta t =$ 1.5 ns, with restrained protein backbone atoms (force constant: 20 kcal/mol Å^2)
	NPγT ensemble, $\delta t = 2$ fs, $\Delta t =$ 2.5 ns, with restrained protein backbone atoms (force constant: 10 kcal/mol Å^2)
	NPγT ensemble, $\delta t = 2$ fs, $\Delta t =$ 0.5 ns, with restrained protein backbone atoms (force constant: 5 kcal/mol Å^2)
	NPγT ensemble, $\delta t = 2$ fs, $\Delta t =$ 0.5 ns, with restrained protein backbone atoms (force constant: 1 kcal/mol Å^2)

theory, and atom centered charges were calculated by means of the RESP module of AMBER8.[43]

After inserting the histamine-hH4R and JNJ7777120-hH4R complexes, minimization, heating, and equilibration were performed using the same protocol (depicted in Table 1), except the runtimes of the discrete equilibration MD steps were set to 0.5 ns. After the restrained equilibration, 20 ns long production runs were performed and analyzed for the native hH4R and the histamine-hH4R and JNJ7777120-hH4R complexes.

For the protein the ff03,[44] for the ligand and POPC molecules the GAFF[45] force field was utilized. The atom types of histamine and JNJ7777120 were allocated using the ANTECHAMBER module[46] of the AMBER8 package. The parameter topology and input coordinate files were generated using the TLEAP module of AMBER8.

During the equilibration and production runs NPγT ($\delta t = 2$ fs) ensemble was used, and the pressure and surface tension were set to 1.01325 bar and 60 dyn/cm, respectively, by means of Langevin dynamics.

During the whole calculation, periodic boundary conditions in all three dimensions were applied. The nonbonded interactions were truncated at 10 Å using a smoothing function from 8 Å and were calculated every step. The long-range electrostatic interactions were calculated using the particle mesh Ewald summation method[47] and were updated in every second step. The evaluation of the trajectory was performed with the PTRAJ module of AMBER9[48] and VMD 1.8.6.[49] Snapshots from the trajectory were aligned with VMD 1.8.6 using the backbone atoms only.

Table 2. Protonation States of Specific Residues and Number of Atoms in Systems I, II, III, and IV

system ID	ligand	Glu160	Glu163	Glu165	no. of atoms
I	no	deprot	prot	prot	67503
II	histamine	prot	prot	prot	67515
III	histamine	prot	prot	deprot	67513
IV	JNJ7777120	deprot	deprot	deprot	67531

3. RESULTS AND DISCUSSION

Protonation State of hH4R Residues. ProPka calculations revealed an unusual protonation state for some residues in hH4R (Table 2). None of these residues are in the transmembrane region; however, Glu165 is in close proximity to histamine in the initial histamine-hH4R complex, and we therefore assumed that the protonation state of this residue can have a significant impact on the results of the MD simulation. Therefore we performed MD simulations with both protonation states of Glu165 (see systems II and III in Table 2).

Equilibration Properties of the Simulations. The potential energy profile of systems I, II, III, and IV in the course of the production run is shown in Figure 3.

The potential energy of the native hH4R (system I) was slowly decreasing until the 10th ns. Then, it remained constant except for a small decrease between 17 and 18.5 ns. In system II the potential energy was stabilized between 4 and 8 ns and then decreased constantly until the 13th ns. It remained stable in the last 9 ns. In contrast to this behavior, the potential energy of system III decreased constantly from the beginning until the 14th ns and remained stable in the last 8 ns. In system IV the potential energy was decreased considerably in the first 10 ns. Then, it remained constant until the 15th ns; after that a rapid significant decrease occurred at 16 ns. In the remaining part of the simulation, the potential energy did not change considerably.

The root-mean-square deviation (rmsd) of the backbone atoms gives information about the structural equilibration of the system (Figure 4).

In system I, the rmsd increased until the 12th ns and then slightly decreased until the 16th ns. Between 17 and 20 ns a significant increase occurred, and the rmsd remained unchanged in the last 5 ns. In system II, the rmsd increased parallel with the decreasing of the potential energy, i.e. it seemed to reach a metastable state between 4 and 8 ns, followed by a constant increase until the 13th ns. After that, the rmsd was stabilized in the last 9 ns. In the case of system III a rapid stabilization of the rmsd was obtained in the first 7 ns, and the rmsd remained stable in the last 15 ns. In the case of system IV the rmsd increased in the first 6 ns, and then after a small decrease it remained constant in the last 12 ns.

Interactions at the Binding Site of the Native hH4R (System I). The binding site of hH4R is predominantly formed by residues of TM3, TM5, and TM6 helices. The most crucial parts of the binding site are Asp94 (3.32) and Glu182 (5.46) based on the available mutagenesis data.[29] During the simulation of the native hH4R, an ionic interaction has been formed between Asp94 (3.32) and the protonated Glu165. This salt bridge remained intact until 18.6

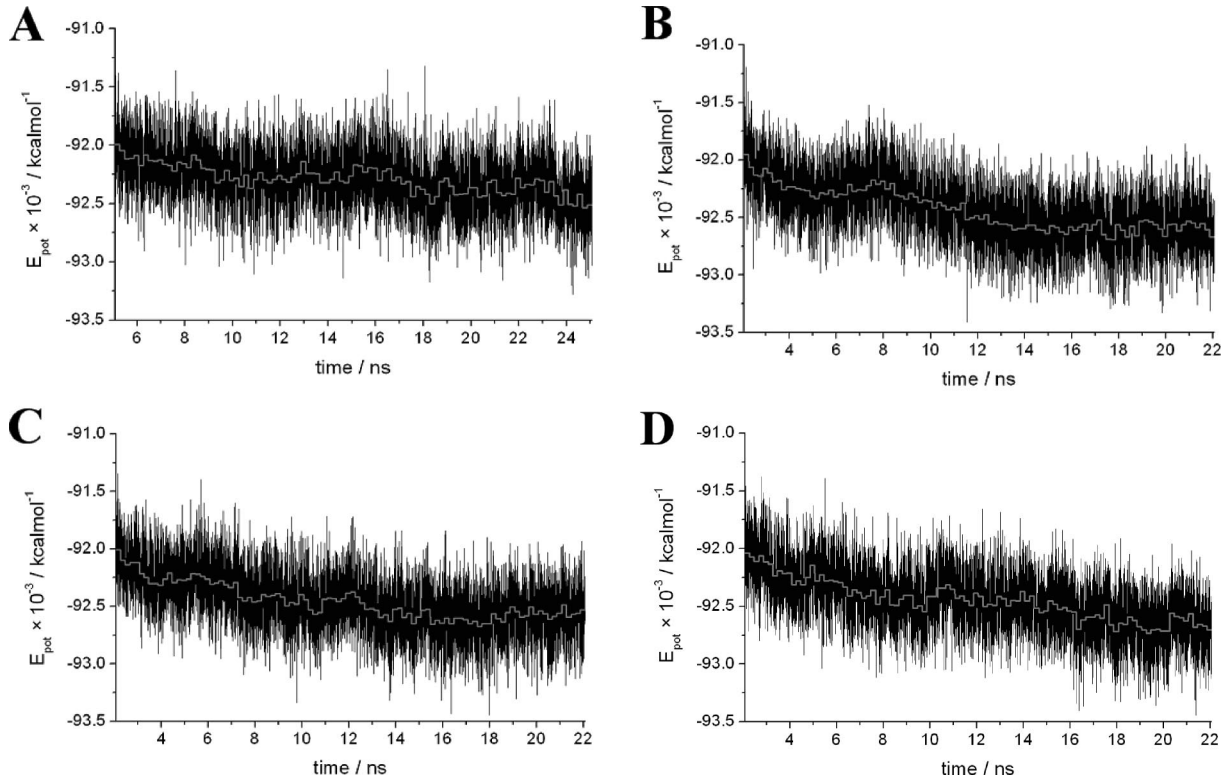

Figure 3. Potential energy vs time plot of the production run of systems I (A), II (B), III (C), and IV (D). The average energy over 200 ps intervals is shown in grey color.

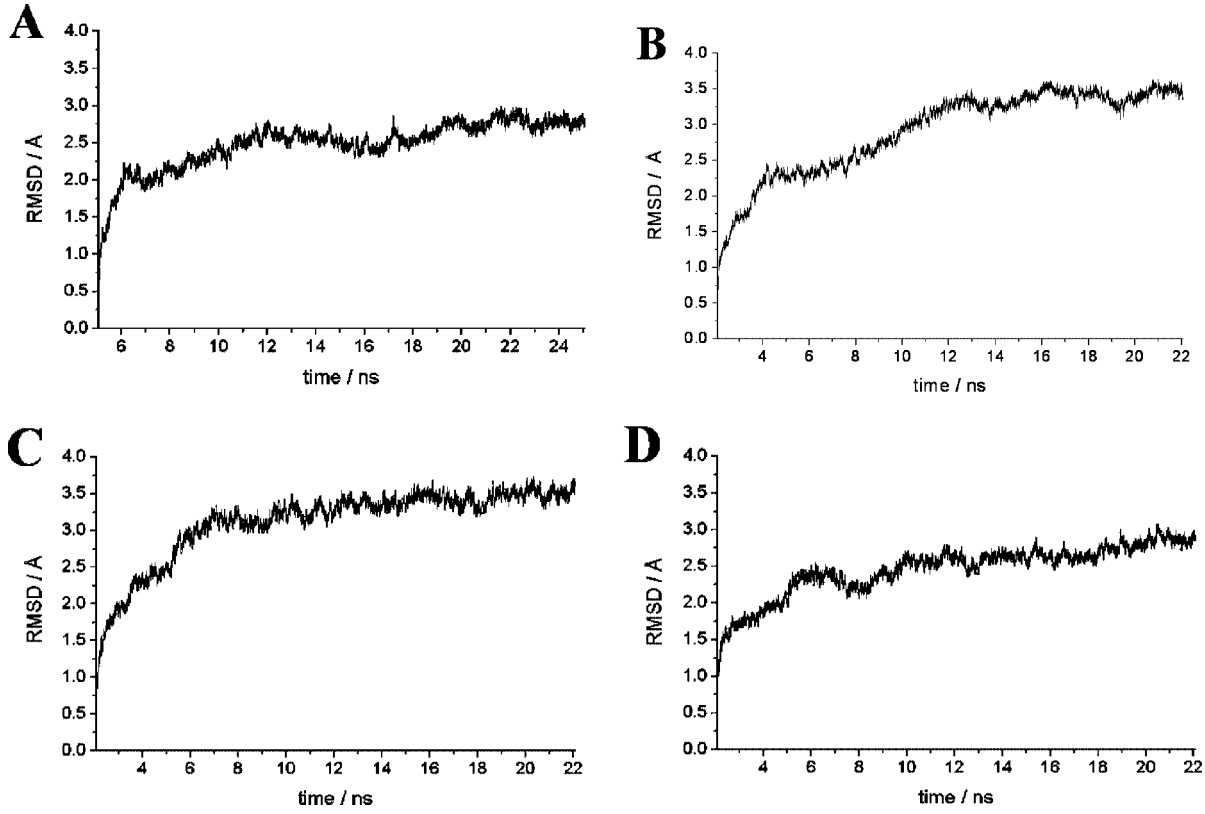

Figure 4. The backbone rmsd vs time plot of the production run of systems I (A), II (B), III (C), and IV (D).

ns, when the side chain of Glu165 turned away. Interestingly, this conformational change overlaps with a significant change in both the potential energy and rmsd between 17 and 19 ns. The two oxygens of the carboxylate group of Glu182 (5.46) were positioned by the hydroxyl groups of Thr99 (3.37) and Ser320 (6.52).

Interactions between Histamine and the hH4R Binding Site (Systems II and III). Shin et al. have shown that Asp94 (3.32) and Glu182 (5.46) are crucial residues in histamine binding.[29] It was also demonstrated that mutations of Thr178 (5.42), Ser179 (5.43), Asn147 (4.57), and Ser320 (6.52) have only a minor effect on histamine binding; on

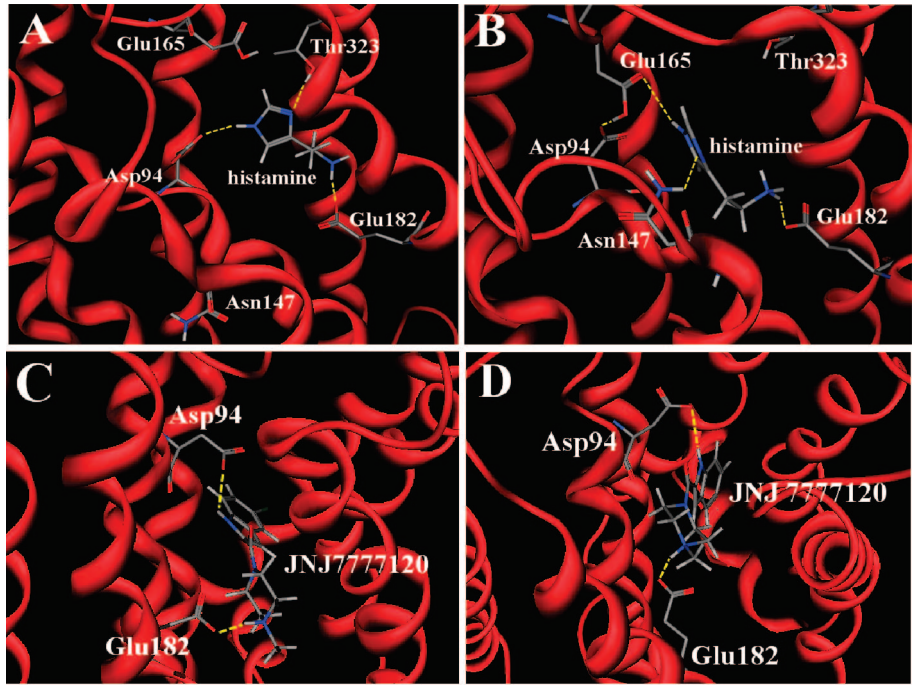

Figure 5. Interactions between histamine and hH4R before (A) and after (B) 22 ns MD simulation (system II). Interactions between JNJ7777120 and hH4R before (C) and after (D) 22 ns MD simulation (system IV). H-bonds and ionic interactions are marked with dashed yellow lines.

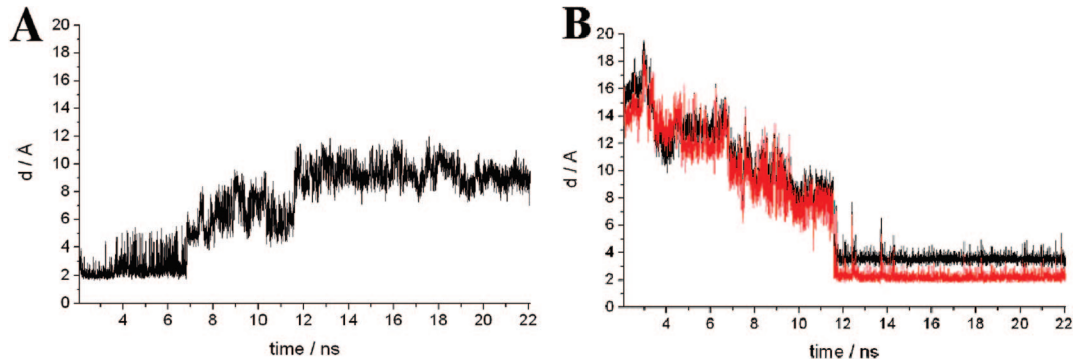

Figure 6. Distances between N(1) of histamine and the hydrogen in the OH group of Thr323 (6.55) (A) and the two hydrogens of the side chain amide group of Asn147 (4.57) (B) during the production run of system II.

the other hand, mutations of Asn147 (4.57) and Ser320 (6.52) have a significant effect on the hH4R activation process. In the initial histamine-hH4R complex the ethylamine side chain of histamine interacts with Glu182 (5.46), the imidazole N(3)-H creates an H-bond with Asp94 (3.32), and an additional H-bond is formed between the imidazole N(1) and Thr323 (6.55) (Figure 5A).

In the case of system II, the interaction between Glu182 (5.46) and the ethylamine side chain of histamine remained intact during the whole simulation. After 1.5 ns, an H-bond has been formed between the protonated Glu165 and Asp94 (3.32). The H-bond between Asp94 (3.32) and N(3)-H of histamine was preserved for quite a long time; however, after 10.2 ns, N(3)-H of histamine created an interaction with the protonated Glu165 instead of Asp94 (3.32). N(3)-H of histamine fluctuated for a while between the two oxygens of the protonated Glu165, but after 12 ns the arrangement depicted in Figure 5B was dominating. Asp94 (3.32) has a key role in the formation of this complex, which is in line with the lost hH4R activity in the absence of this residue.[29]

The interaction between Thr323 (6.55) and N(1) of histamine declined its strength gradually during the simulation (Figure 6A).

Simultaneously, an H-bond between N(1) and Asn147 (4.57) evolved (Figure 6B). This process came to the end at 11.5 ns, when the distance between N(1) and the hydrogen of the side chain amide group of Asn147 (4.57) stabilized around 2 Å. Asn147(4.57)Ala and Asn147(4.57)Tyr mutations cause a 7.5- and a 1.5-fold decrease in hH4R activity, respectively.[29] Since Asn147 (4.57) is an H-bond donor in the above interaction, replacing it with another potential H-bond donor residue exercises only minor influence on hH4R activity. Ser320 (6.52) did not seem to play an important role in the conformational changes occurred during the MD simulation. We found only a weak electrostatic interaction with the protonated ethylamine side chain of histamine during the first nanoseconds, but after 3.6 ns this interaction disappeared. Therefore, we suggest that the affinity and activity changes caused by the Ser320(6.52)Phe mutation[29] are probably the consequence of the binding site perturbation by the bulky Phe residue, rather than the

role of Ser320 (6.52) in ligand binding or receptor activation. This is further supported by the fact that the Ser320(6.52)Ala mutation had only a minor effect on histamine binding or receptor activation.[29] After a 7 ns simulation, Thr178 (5.42) played a role in positioning the ethylamine side chain of histamine. However, the major anchoring interaction at this part of the binding site was the salt bridge between the positively charged ethylamine moiety of histamine and the negatively charged side chain of Glu182 (5.46). This is in agreement with the observation that the Thr178(5.42)Ala mutation only slightly affects histamine binding and hH4R activation. Thr99 (3.37) played a role in positioning the side chain of Glu182 (5.46). This resulted in a highly constrained conformation of the side chain of Glu182 (5.46); therefore, it only rotated two times during the whole simulation (see Figure S2 in the Supporting Information). On the other hand, the hydrogens of the protonated ethylamine of histamine were constantly rotating, indicating a significantly weaker positioning effect of Thr178 (5.42). Dominant interactions between histamine and hH4R after the simulation of system II are depicted in Figure 5B.

In the case of system III, the interaction between the ethylamine side chain of histamine and Glu182 (5.46) remained intact during the simulation. H-bonds with Asp94 (3.32) and Thr323 (6.55), however, vanished after 3.1 ns. N(1) and N(3)-H of histamine did not form any other significant interaction with the binding site during the simulation. Therefore, the interaction pattern of histamine in system III is against either the affinity or the functional data available for hH4R.[29]

In the light of the above results, we conclude that MD simulation of the histamine-hH4R complex, where Glu165 is protonated (system II), reproduced better the available experimental data on hH4R. Furthermore, several other observations in system II—all in line with experimental data on GPCR activation—suggest the activation of hH4R. Therefore, no further analysis of the MD simulation of system III was conducted.

In a recent publication, Ratnala et al. reported that histamine binds to the human histamine H1 receptor (hH1R) in both dicationic and monocationic states.[50] They proposed that after the binding of the dicationic histamine, a proton is transferred to hH1R, and histamine became monocationic. This proton transfer is analogous with that observed in BR, where the proton of the protonated Schiff-base is translocated to Glu113 (3.28) initiating the last part of the activation process. In our histamine-hH4R complexes, histamine is represented in a monocationic form. Besides, ProPka protonation state calculations indicated Glu165 protonated in the initial hH4R complex. We hypothesize that Glu165 may play a similar role as Glu113 (3.28) in BR. Therefore, the simulation with a monocationic histamine and a protonated Glu165 (system II) may correspond to the MII state of BR.

Interactions between JNJ7777120 and the hH4R Binding Site (System IV). In the initial complex of system IV there is a salt bridge between the protonated piperazine moiety of JNJ7777120 and Glu182 (5.46), and the indole NH group forms an H-bond with Asp94 (3.32) (Figure 5C). The salt bridge with Glu182 (5.46) remained stable during the whole MD simulation. In the first part of the simulation, the side chain of Asp94 (3.32) turned away from JNJ7777120 and formed an H-bond with Trp348 (7.43). At this time, the backbone oxygen of Asp94 (3.32) interacted with the indole NH group of JNJ7777120. At 8.3 ns, the side chain of Gln347 (7.42) moved in the direction of Asp94 (3.32). Consequently, Asp94 (3.32) turned back and created an H-bond with Gln347 (7.42). In this orientation, the formation of the H-bond between JNJ7777120 and Asp94 (3.32) was also possible, and it was indeed established at 9.2 ns. This H-bond was preserved during the rest of the simulation (Figure 5D).

Comparison of the MD Simulations with Literature Data on GPCR Activation. BR is the most extensively studied member of the GPCR superfamily, with several valuable observations about its activation mechanism. The ligand of inactive BR is 11-cis retinal that is covalently linked to Lys296 (7.43) via a protonated Schiff-base. Upon light exposure, BR is activated by forming several transition states, i.e. bathorhodopsin, lumirhodopsin, metarhodopsin I (MI), metarhodopsin IIa (MIIa), and metarhodopsin IIb (MIIb). The primary step of the activation is the isomerization of 11-cis retinal to all-trans retinal that happens in femtoseconds.[51] The formation of bathorhodopsin, lumirhodopsin, and MI take microseconds.[52] Based on the experimental data, no large structural rearrangements are apparent until the MI state.[52] After MI, the proton of the Schiff-base is transferred to Glu113 (3.28) (MIIa), followed by the uptake of another proton from the IC side by Glu134 (3.49). It is postulated that this proton uptake results in the disintegration of the ionic lock between Arg135 (3.50) and Glu247 (6.30) (MIIb). This conversion takes milliseconds. Since MD simulations are usually performed on a nanosecond time scale, only some of the initial steps of BR activation can be investigated by traditional MD approaches. Although, some techniques exist that can facilitate helix movements,[53,54] the need for microsecond simulation is obvious to study late events of BR activation. On the other hand, there are several significant differences between BR and other GPCRs. In particular, the constitutive activity of BR is practically zero, which is in relation with its biological function—rhodopsin should remain in the inactive state in the absence of light. This is provided by several interhelical interactions that serve as potential energy barriers. Probably the most important stabilizing lock in BR is composed by Arg135 (3.50) and Glu247 (6.30) that diminishes upon formation of MIIb. This interaction stabilizes the distance of the IC part of TM3 and TM6. Experimental data suggest the movement of the cytoplasmic ends of TM3 and TM6 relative to each other during activation,[19,20] which further supports the proposed role of the above-mentioned ionic lock. Some other GPCRs, however, were found to possess reasonable constitutive activity, suggesting a less hampered formation of the active state, comparing with that of BR. For example, the constitutively active CCR5 contains an Arg instead of an acidic residue at the 6.30 position. Mutational analyses on CCR5 revealed that displacement of Arg (6.30) to Asp or Glu results in an almost silent receptor, devoid of constitutive activity.[55] This result demonstrates that the wild-type CCR5 lacks the ionic lock between TM3 and TM6. The recently solved crystal structures of the partially activated hβ2AR also lack this salt bridge between TM3 and TM6.[4,5] In the case of hH4R, the 6.30 position is occupied by an Ala residue, suggesting that hH4R also lacks the above-mentioned ionic lock. In fact, hH4R possesses high constitutive activity. Considering this,

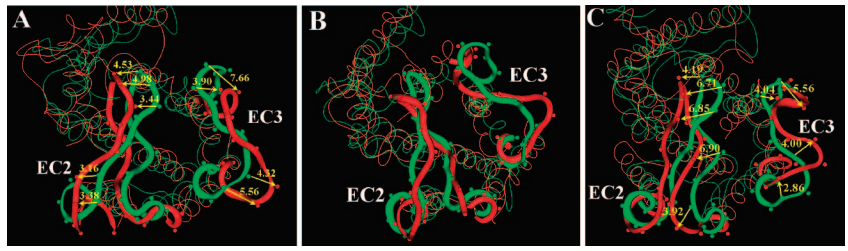

Figure 7. EC2 and EC3 backbone of the histamine-hH4R complex (A), the native hH4R (B), and the JNJ7777120-hH4R complex (C) in the first (green) and the last (red) frame of the production run are shown as tube representation. Other parts of the backbone are shown as line representation. Distances between equivalent C-alpha atoms in Ångström are depicted in yellow color.

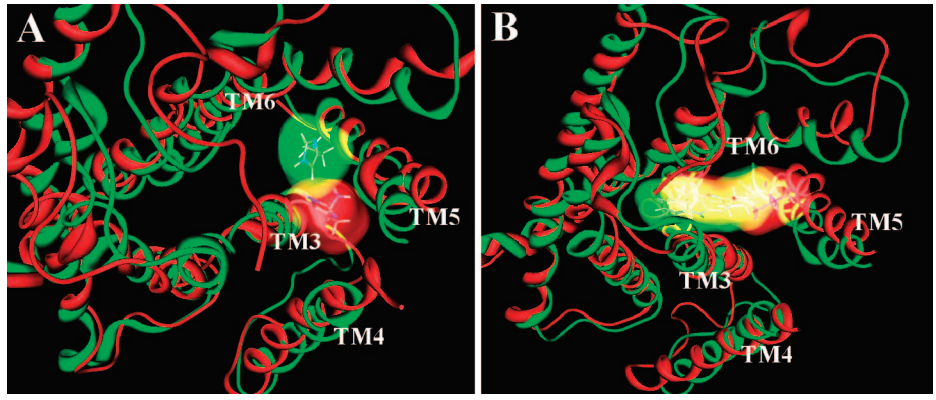

Figure 8. Movement of histamine (A) and JNJ7777120 (B) at the binding site of hH4R viewing from the EC side. The backbones of hH4R in the first (green) and the last (red) frame of the production run are shown as tube representation, except EC2, that is not shown for clarity. Histamine and JNJ7777120 are represented by stick rendering, with their molecular surface in the first (green) and the last (red) frame of the production run. Overlapping molecular surfaces appear in yellow color.

and the fact that the most time-consuming part of BR activation is the disruption of the ionic lock between Arg135 (3.50) and Glu247 (6.30), it seems possible to analyze the hH4R activation mechanism with MD simulation in a membrane environment.

Movements of EC2 and EC3. In the simulation of the histamine-hH4R complex (system II), the second (EC2) and the third (EC3) extracellular loops moved in such a manner that the binding site became wider and more accessible from the EC side (Figure 7A).

A similar movement of EC2 and EC3 was found in the simulation of the JNJ7777120-hH4R complex (Figure 7C). Interestingly, no such movement was observed in the case of the native hH4R (Figure 7B). We suggest that in the presence of a ligand, hH4R adopts a significantly opened binding site. This is maybe partially the consequence of homology modeling based on the BR template, since EC2 of BR folds down deeply and forms direct interactions with retinal. Accordingly, BR has a rather closed and small binding site. In the case of the native hH4R there are no conformational strains at the binding site; however, in the presence of a ligand, EC2 and EC3 loops have to move outward to properly accommodate the ligand. In line with this hypothesis, the EC2 loop in the crystal structure of the carazolol bound hβ2AR possesses a remarkably more opened folding than that of BR. Moreover, the EC3 loop of hβ2AR is positioned outward comparing it with that of BR.

Water Influx at the Binding Site. In our simulations, several water molecules flew into the binding site from the extracellular milieu. As a consequence of the outward movement of the EC loops, this water influx was more expressed in the case of the histamine-hH4R and JNJ7777120-hH4R complexes. These waters were involved in the interactions between the ligands and the hH4R binding site (see Figure S3 in the Supporting Information). These waters were not essential for maintaining the interactions between the ligands and hH4R; however, they stabilized the previously formed interactions. Our observations are also in line with the experiences of Henin et al.[14] These authors have simulated the human cholecystokinin-1 receptor in complex with an agonist ligand in an explicit membrane environment. They found that a water cluster was formed in the binding cavity over a period of 3 ns, and these waters exchanged rapidly, especially near the EC part of the binding site. They also found a complementary role of the waters at the binding site, filling available vacuities and solvating moieties of the ligand. In another study, Rivail et al. report the MD simulation of the human 5-HT4 receptor in complex with an antagonist in a lipid bilayer.[16] They also found several water molecules migrating from the extracellular milieu to the binding pocket.

Ligand Movement. Experimental data indicate that the β-ionine ring of retinal gets closer to TM3 and TM4 upon BR activation.[56] This is further supported by the study of Borhan et al.[57] Here, authors report that the β-ionine ring gets closer to Ala169 (4.58) in TM4 at the later stages of BR activation. At the same time, it moves away from Trp265 (6.48) a residue in TM6. In the MD simulation of system II, histamine considerably changed its position at the binding site (Figure 8A).

This change in ligand position started after 6 ns and took approximately until 12 ns. The largest movements of histamine were attained in the direction of TM3 and TM4 and away from TM6. Gly148 (4.58) occupies the same position in our model as Ala169 (4.58) in BR. This residue is far away from histamine at the beginning of the production run, i.e. the distance between their closest atoms is 9.97 Å

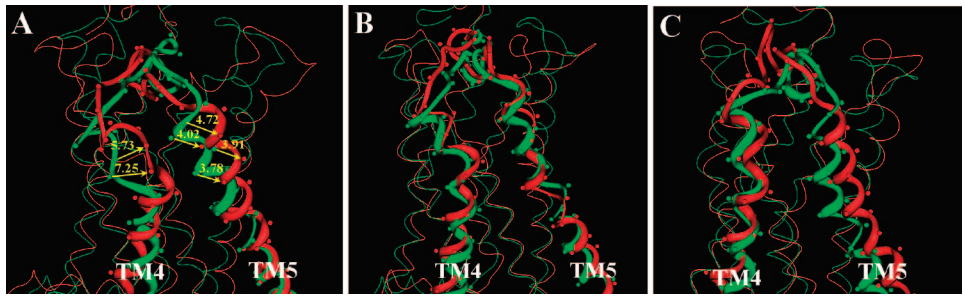

Figure 9. Movement of the EC part of TM4 and TM5 in the histamine-hH4R complex (A), in the native hH4R (B), and in the JNJ7777120-hH4R complex (C). The backbone of TM4, TM5, and EC2 in the first (green) and the last (red) frame of the production runs are shown as tube representation. Other parts of the backbone are shown as line representation. Distances between equivalent C-alpha atoms in Ångström are depicted in yellow color.

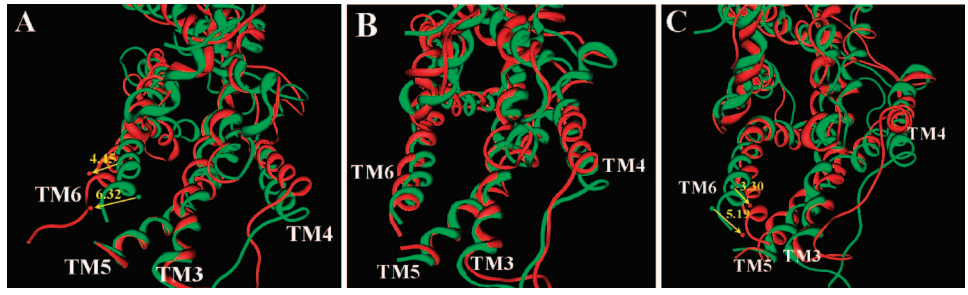

Figure 10. IC side of the histamine-hH4R complex (A), the native-hH4R (B), and the JNJ7777120-hH4R complex (C). The backbone of hH4R in the first (green) and the last (red) frame of the production run is shown as tube representation. Distances between equivalent C-alpha atoms in Ångström are depicted in yellow color.

(see Figure S4A in the Supporting Information). However, in the last frame of the simulation this distance is 5.81 Å. It is important to mention that the sequence homology at the EC part of TM4 between hH4R and BR is reasonably low; therefore, it is possible that the position of Ala169 (4.58) is properly aligned with Asn147 (4.57) in hH4R. The closest distance between Asn147 (4.57) and histamine is 8.22 Å in the first frame of the production run (see Figure S4A in the Supporting Information). This distance is continuously decreasing, and after 11.5 ns an H-bond is formed between the amide group of Asn147 (4.57) and N(1) of histamine (Figure 6B). The equivalent of the BR residue Trp265 (6.48) is Trp316 (6.48) in hH4R. This residue is in close contact with histamine at the beginning: the shortest distance is 2.20 Å (see Figure S4A in the Supporting Information). However, histamine moved away from TM6 during the simulation, and the distance increased to 6.45 Å. We suggest that the movement of histamine away from TM6 may result in a higher level of conformational freedom of this helix, which facilitates the helical movements leading to receptor activation. In contrast to these results JNJ7777120 did not change its position considerably during the simulation (Figure 8B; see also Figure S4B in the Supporting Information).

Rearrangement of the EC Side of TM4 and TM5. At the EC side, the distance between the equivalent C-alpha atoms in the first and the last frame of the production run of the histamine-hH4R complex deviates in TM4 to the highest degree. The EC region of TM4 underwent a significant rearrangement during the simulation, and it moved together with TM5 (Figure 9A).

Guo et al. have shown that a conformational change at the TM4 dimer interface is part of the D2 receptor activation process.[58] In our histamine-hH4R simulation, a significant increase in the rmsd values was observed in the EC part of TM4 between 7 and 12 ns (see Figure S5D in the Supporting Information). We suggest that the rearrangement of the EC part of TM4 is maybe associated with the transformation of the dimeric interface of hH4R, although a long lasting simulation of a dimer hH4R complex should be performed to test this hypothesis. Interestingly, no such helix rearrangement was found during the simulation of the native hH4R (Figure 9B). In the case of the JNJ7777120-hH4R complex, only the movement of TM5 was observed, but this shift concerned not only the EC part of the helix (Figure 9C).

Movement of the EC Side of TM3. The recent publication of Salom et al. indicates that the middle of TM3 in the photoactivated BR is quite mobile.[59] In this BR structure the ionic lock between Arg135 (3.50) and Glu247 (6.30) is weakened but still exists; therefore, it represents the MIIa state. Nakamichi et al. reported that during the transformation of bathorhodopsin to lumirhodopsin, a significant peptide displacement can be observed in the middle of TM3, including approximately two helical turns.[58] During the MD simulation of the histamine-hH4R complex, two or three helical turns in TM3 moved outward. This outward movement was, however, closer to the EC part of TM3, rather than in the middle of the helix (see Figure S6A in the Supporting Information). It is also important to mention that we found a slight inward movement in the case of the JNJ7777120-hH4R complex and a more expressed inward movement in the native hH4R simulation (see Figure S6C and S6B, respectively in the Supporting Information).

Movement of the IC Side of TM6. Farrens et al. found that photoactivation of BR induces a movement of the IC ends of TM3 and TM6.[19] In the histamine-hH4R simulation, we found significant changes on the IC side between TM3 vs TM6 and TM6 vs TM7 (Figure 10A).

Both of these were mainly caused by the movement of the IC part of TM6. The largest movement of TM6 was observed between 8 and 11 ns (see Figure S7A in the

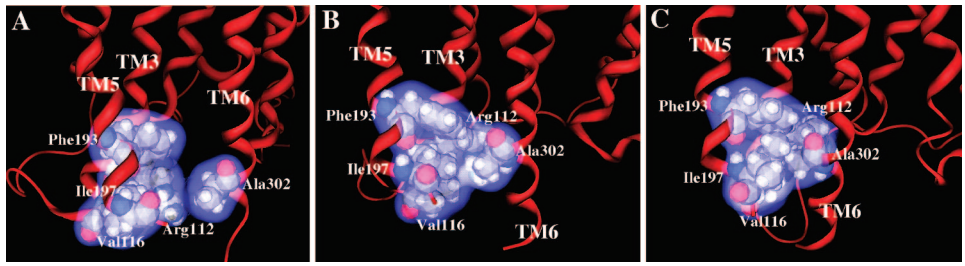

Figure 11. Lipophilic microdomain comprised of residues of TM3, TM5, and TM6 is shown in the last frame of the production run of the histamine-hH4R complex (A), the native hH4R (B), and the JNJ7777120-hH4R complex (C). Residues are shown as space filling representation, with their blue colored van der Waals surfaces. Backbone is shown as tube representation.

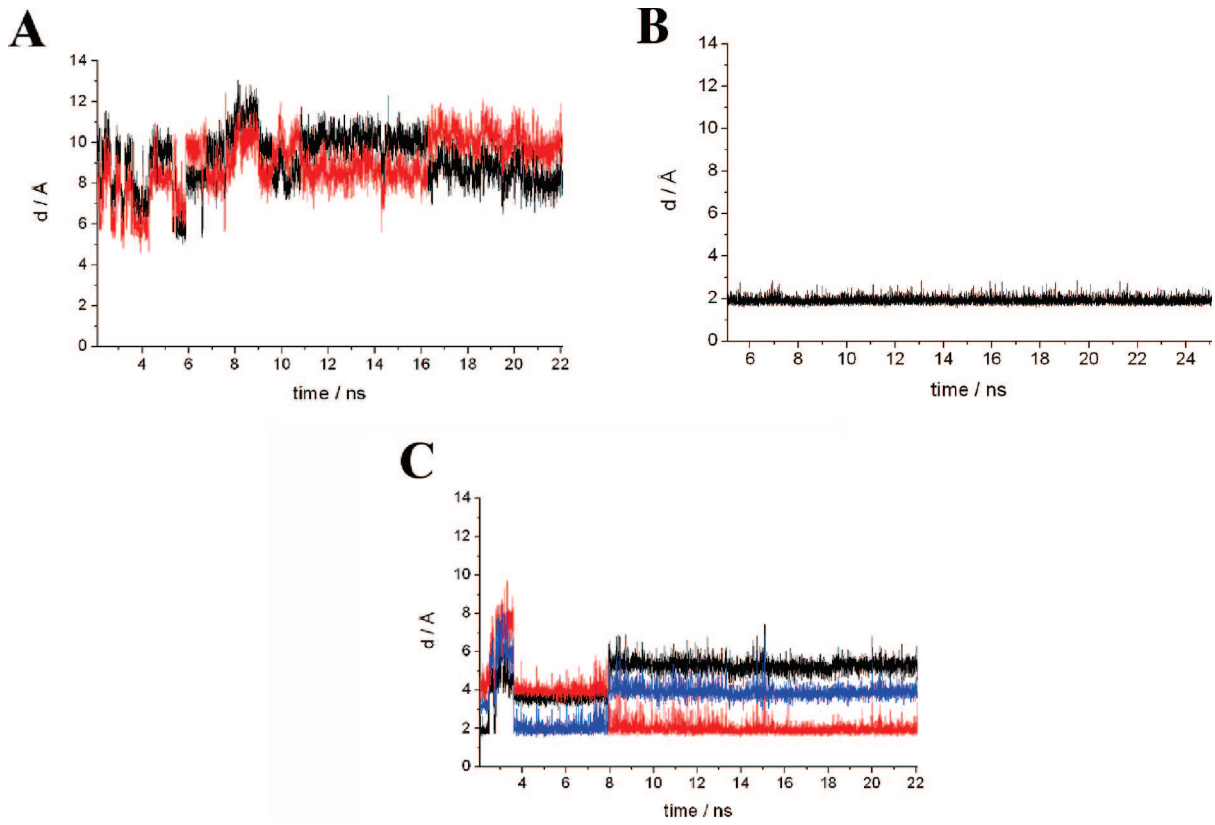

Figure 12. Distance between the closest side chain oxygen atom(s) of Asp111 (3.49) and the closest hydrogen atom(s) of the side chain of Arg112 (3.50) in the histamine-hH4R complex (A), in the native hH4R (B), and in the JNJ7777120-hH4R complex (C).

Supporting Information), when the rmsd of the system was constantly increasing, and the potential energy was constantly decreasing (Figures 3B and 4B, respectively). The movement of the IC part of TM6 was not as large as Farrens et al. reported for BR; however, its direction away from TM3 and TM7 is in good agreement with the proposed inactive and active BR models of Farrens et al.[19] Interestingly, no such movement of TM6 was found during the simulation of the native hH4R (Figure 10B). Moreover, a significant movement of the IC side of TM6 in the direction of TM3 was observed in the case of the JNJ7777120-hH4R complex (Figure 10C). In the hβ2AR crystal structures the IC end of TM6 is slightly positioned outward compared with that of BR; however, the movement of this region in our histamine-hH4R complex is much more extensive. This is in agreement with the hypothesis that the crystal structure of BR and hβ2AR represents an inactive and a partially activated GPCR, respectively, while our MD simulation in the presence of histamine resulted in activated state.

Movement of the IC Side of TM4. In all three simulations, the IC part of TM4 showed a significant divergence from its initial position. The direction of these movements was similar. BR has an additional Pro residue in TM4 compared to that of hH4R. Therefore, we suggest that conformational strains in TM4 caused by the homology modeling based on the BR template are relaxed during the MD simulations (see Figure S5A−C in the Supporting Information).

Interhelical Interactions at the IC Side of TM3, TM5, and TM6. In the initial histamine-hH4R complex, Arg112 (3.50) of the DRY motif formed an H-bond with the backbone oxygen of Ala298 (6.30). This Ala residue occupies the same position as Glu247 (6.30) in BR; therefore, we suggested that it might play a similar role. This interaction in hH4R is, however, significantly weaker, and it lost its strength at the beginning of the simulation. In the native hH4R and in the JNJ7777120-hH4R complex there is no interaction between Arg112 (3.50) and Ala298 (6.30).

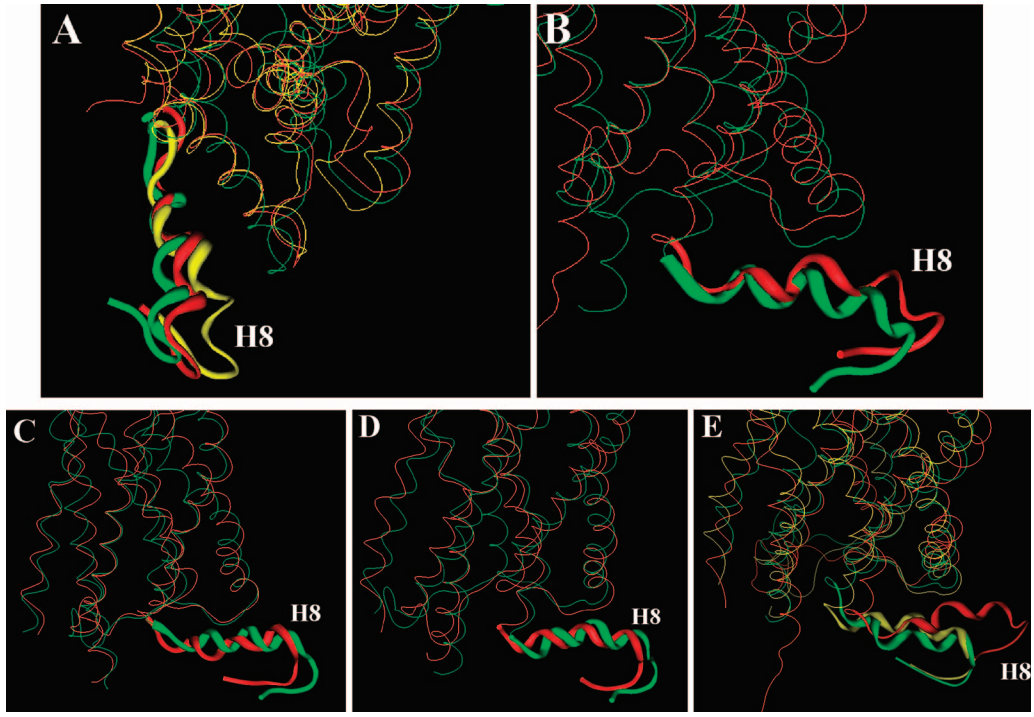

Figure 13. Movement of H8 during the MD simulation. The backbone of H8 is shown as tube representation; other parts of the backbone are shown as line representation. The histamine-hH4R complex in the initial frame (green), after 11.5 ns simulation (yellow), and in the last frame (red) of the production run (A). The histamine-hH4R complex in the initial frame (green) and in the last frame (red) of the production run (B). The native hH4R in the initial frame (green) and in the last frame (red) of the production run (C). The JNJ7777120-hH4R complex in the initial frame (green) and in the last frame (red) of the production run (D). The native hH4R (green), the histamine-hH4R complex (red), and the JNJ7777120-hH4R complex (yellow) in the last frame of the production run (E).

Therefore we concluded that−similarly to the CCR5 receptor−this interhelical interaction is missing in hH4R.

In the recently published crystal structures of the partially activated hβ2AR the ionic interaction between TM3 and TM6 is also missing.[4,5] On the other hand, Leu272 (6.34) in hβ2AR forms a lipophilic microdomain together with residues in TM3 and TM5.[4] Therefore it is assumed that this domain stabilizes the inactive conformation of the receptor.[4] Surprisingly, this is in full agreement with our results, since we found that Ala302 (6.34), which is the equivalent of Leu272 (6.34) in hβ2AR, participates in such a stabilizing lipophilic domain in the native hH4R and is even more expressed in the JNJ7777120-hH4R complex (Figure 11).

This domain is comprised of Val116 (3.54), Phe193 (5.57), Ile197 (5.61), the side chain carbons of Arg112 (3.50), and Ala302 (6.34). Residues in TM3 and TM5 form a "lock", and Ala302 (6.34) seems to fit perfectly into this "lock" in the JNJ7777120-hH4R complex. In the native hH4R, Ala302 (6.34) is positioned slightly farther from this motif, but it is still close enough to evolve some strong lipophilic interactions. In the histamine-hH4R complex, however, Ala302 (6.34) is found even farther from this lipophilic microdomain. Considering that van der Waals attractive forces are inversely proportional to the sixth power of separation, Ala302 (6.34) only forms weak interactions with the lipophilic domain in the histamine-hH4R complex. These results suggest the inactive state stabilizing role of this lipophilic microdomain of hH4R, which was found to be partially disrupted in the active state.

Interaction between the Conserved Asp111 (3.49) and Arg112 (3.50). In the crystal structures of the inactive BR, there is a strong ionic interaction between Glu134 (3.49) and Arg135 (3.50). The distance between the corresponding heavy atoms is 2.85 Å (PDB ID: 1U19). In the photoactivated BR this interaction is weakened, as this distance is 3.46 Å (PDB ID: 2I37). Although, it has to be mentioned that the crystal structure of the photoactivated BR was solved at only 4.15 Å resolution. In the recently solved crystal structure of the partially activated hβ2AR (PDB ID: 2RH1), the distance between the corresponding heavy atoms of Asp130 (3.49) and Arg131 (3.50) is 3.46 Å. These data suggest that impairment of this salt bridge is a characteristic sign of GPCR activation. In the case of the histamine-hH4R simulation this interaction was completely missing during the whole simulation (Figure 12A).

In the simulation of the native hH4R and the JNJ7777120-hH4R complex the distance of Asp111 (3.49) and Arg112 (3.50) fluctuated around 2 Å during the whole simulation (parts B and C, respectively, of Figure 12), suggesting the dominance of the inactive state of the receptor.

Movement of H8. In the histamine-hH4R simulation a considerable change was observed in H8. Namely, the C-terminal of H8 moved in the direction of TM1 between 7.5 and 11 ns (Figure 13A) (see also Figure S8 in the Supporting Information).

This overlaps with the movement of the IC end of TM6 between 8 and 13 ns. After that, H8 moved backward; however, its length was elongated considerably compared to that in the initial state. In the case of the native hH4R and the JNJ7777120-hH4R complex, H8 showed less extensive movements during the simulation; however, H8 became significantly shorter than in the initial frame (Figure 13C,D). The difference in the conformation of H8 is even more conspicuous if we align the last frames of the native

hH4R, the histamine-hH4R complex, and the JNJ7777120-hH4R complex simulations (Figure 13E).

4. CONCLUSIONS

In conclusion, we carried out a membrane-embedded molecular dynamics simulation of hH4R alone, in complex with its natural agonist histamine and a selective antagonist JNJ7777120. Our results are in agreement with the available mutagenesis data on hH4R as well as several experimental data on GPCR activation. In particular, histamine formed an H-bond with Asn147 (4.57) that was previously proved to be important for hH4R activation.[29] We found that the IC part of TM6 moved outward relative to TM3 and TM7 in the histamine-hH4R simulation. On the other hand, a significant movement of TM6 in the opposite direction could be observed in the case of the JNJ7777120-hH4R simulation. Several observations suggest that the native hH4R and the JNJ7777120-hH4R simulations resulted in an inactive receptor state. In the presence of histamine, however, our receptor model seems to be in its active state. Interestingly, most of the changes in the histamine-hH4R complex happened between 8 and 13 ns of the simulation, in parallel with the significant decrease of potential energy and increase of the rmsd of the system. In our opinion, snapshots of the dynamics can be used in structure-based drug design to find novel hH4R ligands.

Abbreviations: GPCR, G-protein-coupled receptor; hH4R, human histamine H4 receptor; H3R, histamine H3 receptor; hH1R, human histamine H1 receptor; BR, bovine rhodopsin; CNS, central nervous system; TM, transmembrane; EC, extracellular; IC, intracellular; H8, helix 8; rmsd, root-mean-square deviation; POPC, 1-palmitoyl-2-oleoyl-phosphatidylcholine; TIP3P, transferable intermolecular potential 3P; MD, molecular dynamics; CCR5, CC chemokine receptor CCR5; hβ2AR, human β2 adrenergic receptor.

ACKNOWLEDGMENT

The financial support provided by the Grant OTKA (T 042933) from the Hungarian National Research Fund is gratefully acknowledged. One of the authors (B.V.) thanks the National Office for Research and Technology for the Öveges Research Program (HEF_06_1-PESINF06). The authors thank Máté Labádi for technical support at the HPC Centre of the University of Szeged.

Supporting Information Available: Figures from different perspectives about hH4R alone and in complex with histamine and JNJ7777120 and distance data between the corresponding atoms involved in specific H-bonds and between C-alpha atoms of specific residues, and mutational data available for hH4R from the literature. This material is available free of charge via the Internet at http://pubs.acs.org.

REFERENCES AND NOTES

(1) Takeda, S.; Kadowaki, S.; Haga, T.; Takaesu, H.; Mitaku, S. Identification of G protein-coupled receptor genes from the human genome sequence. *FEBS Lett.* **2002**, *520*, 97–101.
(2) Lundstrom, K. Structural genomics of GPCRs. *Trends Biotechnol.* **2005**, *23*, 103–108.
(3) Palczewski, K. K.; Kumasaka, T.; Hori, T.; Behnke, C. A.; Motoshima, H.; Fox, B. A.; Le Trong, I.; Teller, D. C.; Okada, T.; Stenkamp, R. E.; Yamamoto, M.; Miyano, M. Crystal structure of rhodopsin: A G protein-coupled receptor. *Science* 2000*289*, 739–745.
(4) Rasmussen, S. G.; Choi, H. J.; Rosenbaum, D. M.; Kobilka, T. S.; Thian, F. S.; Edwards, P. C.; Burghammer, M.; Ratnala, V. R.; Sanishvili, R.; Fischetti, R. F.; Schertler, G. F.; Weis, W. I.; Kobilka, B. K. Crystal structure of the human beta2 adrenergic G-protein-coupled receptor. *Nature* **2007**, *450*, 383–387.
(5) Cherezov, V.; Rosenbaum, D. M.; Hanson, M. A.; Rasmussen, S. G.; Thian, F. S.; Kobilka, T. S.; Choi, H. J.; Kuhn, P.; Weis, W. I.; Kobilka, B. K.; Stevens, R. C. High-resolution crystal structure of an engineered human beta2-adrenergic G protein-coupled receptor. *Science* **2007**, *318*, 1258–1265.
(6) Furse, K. E.; Lybrand, T. P. Three-dimensional models for beta-adrenergic receptor complexes with agonists and antagonists. *J. Med. Chem.* **2003**, *46*, 4450–4462.
(7) Costanzi, S.; Mamedova, L.; Gao, Z. G.; Jacobson, K. A. Architecture of P2Y nucleotide receptors: structural comparison based on sequence analysis, mutagenesis, and homology modeling. *J. Med. Chem.* **2004**, *47*, 5393–5404.
(8) Salo, O. M.; Lahtela-Kakkonen, M.; Gynther, J.; Jarvinen, T.; Poso, A. Development of a 3D model for the human cannabinoid CB1 receptor. *J. Med. Chem.* **2004**, *47*, 3048–3057.
(9) ter Laak, A. M.; Timmerman, H.; Leurs, R.; Nederkoorn, P. H.; Smit, M. J.; Donne-Op den Kelder, G. M. Modelling and mutation studies on the histamine H1-receptor agonist binding site reveal different binding modes for H1-agonists: Asp116 (TM3) has a constitutive role in receptor stimulation. *J. Comput.-Aided Mol. Des* **1995**, *9*, 319–330.
(10) Clark, D. E.; Higgs, C.; Wren, S. P.; Dyke, H. J.; Wong, M.; Norman, D.; Lockey, P. M.; Roach, A. G. A virtual screening approach to finding novel and potent antagonists at the melanin-concentrating hormone 1 receptor. *J. Med. Chem.* **2004**, *47*, 3962–3971.
(11) Evers, A.; Klebe, G. Successful virtual screening for a submicromolar antagonist of the neurokinin-1 receptor based on a ligand-supported homology model. *J. Med. Chem.* **2004**, *47*, 5381–5392.
(12) Evers, A.; Klabunde, T. Structure-based drug discovery using GPCR homology modeling: successful virtual screening for antagonists of the alpha1A adrenergic receptor. *J. Med. Chem.* **2005**, *48*, 1088–1097.
(13) Varady, J.; Wu, X.; Fang, X.; Min, J.; Hu, Z.; Levant, B.; Wang, S. Molecular modeling of the three-dimensional structure of dopamine 3 (D3) subtype receptor: discovery of novel and potent D3 ligands through a hybrid pharmacophore- and structure-based database searching approach. *J. Med. Chem.* **2003**, *46*, 4377–4392.
(14) Henin, J.; Maigret, B.; Tarek, M.; Escrieut, C.; Fourmy, D.; Chipot, C. Probing a model of a GPCR/ligand complex in an explicit membrane environment: the human cholecystokinin-1 receptor. *Biophys. J.* **2006**, *90*, 1232–1240.
(15) Hallmen, C.; Wiese, M. Molecular dynamics simulation of the human adenosine A3 receptor: agonist induced conformational changes of Trp243. *J. Comput.-Aided Mol. Des.* **2006**, *20*, 673–684.
(16) Rivail, L.; Chipot, C.; Maigret, B.; Bestel, I.; Sicsic, S.; Tarek, M. Large-scale molecular dynamics of a G protein-coupled receptor, the human 5-HT4 serotonin receptor, in a lipid bilayer. *J. Mol. Struct. (Theochem)* **2007**, *817*, 19–26.
(17) Schlegel, B.; Laggner, C.; Meier, R.; Langer, T.; Schnell, D.; Seifert, R.; Stark, H.; Höltje, H. D.; Sippl, W. Generation of a homology model of the human histamine H(3) receptor for ligand docking and pharmacophore-based screening. *J. Comput.-Aided Mol. Des.* **2007**, *21*, 437–453.
(18) Zhang, Y.; Sham, Y. Y.; Rajamani, R.; Gao, J.; Portoghese, P. S. Homology modeling and molecular dynamics simulations of the mu opioid receptor in a membrane-aqueous system. *ChemBioChem* **2005**, *6*, 853–859.
(19) Farrens, D. L.; Altenbach, C.; Yang, K.; Hubbell, W. L.; Khorana, H. G. Requirement of rigid-body motion of transmembrane helices for light activation of rhodopsin. *Science* **1996**, *274*, 768–770.
(20) Hubbell, W. L.; Altenbach, C.; Hubbell, C. M.; Khorana, H. G. Rhodopsin structure, dynamics, and activation: a perspective from crystallography, site-directed spin labeling, sulfhydryl reactivity, and disulfide cross-linking. *Adv. Protein Chem.* **2003**, *63*, 243–290.
(21) Liu, C.; Ma, X.; Jiang, X.; Wilson, S. J.; Hofstra, C. L.; Blevitt, J.; Pyati, J.; Li, X.; Chai, W.; Carruthers, N.; Lovenberg, T. W. Cloning and pharmacological characterization of a fourth histamine receptor (H(4)) expressed in bone marrow. *Mol. Pharmacol.* **2001**, *59*, 420–426.
(22) Morse, K. L.; Behan, J.; Laz, T. M.; West, R. E.; Greenfeder, S. A.; Anthes, J. C.; Umland, S.; Wan, Y.; Hipkin, R. W.; Gonsiorek, W.; Shin, N.; Gustafson, E. L.; Qiao, X.; Wang, S.; Hedrick, J. A.; Greene, J.; Bayne, M.; Monsma, F. J. Cloning and characterization of a novel human histamine receptor. *J. Pharmacol. Exp. Ther.* **2001**, *296*, 1058–1066.
(23) Hofstra, C. L.; Desai, P. J.; Thurmond, R. L.; Fung-Leung, W. P. Histamine H4 receptor mediates chemotaxis and calcium mobilization of mast cells. *J. Pharmacol. Exp. Ther.* **2003**, *305*, 1212–1221.

(24) Lippert, U.; Artuc, M.; Grutzkau, A.; Babina, M.; Guhl, S.; Haase, I.; Blaschke, V.; Zachmann, K.; Knosalla, M.; Middel, P.; Kruger-Krasagakis, S.; Henz, B. M. Human skin mast cells express H2 and H4, but not H3 receptors. *J. Invest. Dermatol.* **2004**, *123*, 116–123.
(25) Voehringer, D.; Shinkai, K.; Locksley, R. M. Type 2 immunity reflects orchestrated recruitment of cells committed to IL-4 production. *Immunity* **2004**, *20*, 267–277.
(26) Buckland, K. F.; Williams, T. J.; Conroy, D. M. Histamine induces cytoskeletal changes in human eosinophils via the H(4) receptor. *Br. J. Pharmacol.* **2003**, *140*, 1117–1127.
(27) Ling, P.; Ngo, K.; Nguyen, S.; Thurmond, R. L.; Edwards, J. P.; Karlsson, L.; Fung-Leung, W. P. Histamine H4 receptor mediates eosinophil chemotaxis with cell shape change and adhesion molecule upregulation. *Br. J. Pharmacol.* **2004**, *142*, 161–171.
(28) Ballesteros, J. A.; Weinstein, H. Integrated methods for the construction of three-dimensional models and computational probing of structure-function relations in G protein-coupled receptors. *Methods Neurosci.* **1995**, *25*, 366–428.
(29) Shin, N.; Coates, E.; Murgolo, N. J.; Morse, K. L.; Bayne, M.; Strader, C. D.; Monsma, F. J. Molecular modeling and site-specific mutagenesis of the histamine-binding site of the histamine H4 receptor. *Mol. Pharmacol.* **2002**, *62*, 38–47.
(30) Kiss, R.; Noszál, B.; Rácz, Á.; Falus, A.; Erős, D.; Keserű, G. M. Binding mode analysis and enrichment studies on homology models of the human histamine H4 receptor. Eur. J. Med. Chem. (In Press)
(31) Schlegel, B.; Sippl, W.; Höltje, H. D. Molecular dynamics simulations of bovine rhodopsin: influence of protonation states and different membrane-mimicking environments. *J. Mol. Model.* **2005**, *12*, 49–64.
(32) Ramirez, F. J.; Tunon, I.; Collado, J. A.; Silla, E. Structural and vibrational study of the tautomerism of histamine free-base in solution. *J. Am. Chem. Soc.* **2003**, *123*, 2328–2340.
(33) Collado, J. A.; Tunon, I.; Silla, E.; Ramirez, F. J. Vibrational dynamics of histamine monocation in solution: an experimental (FT-IR, FT-Raman) and theoretical (SCRF-DFT) study. *J. Phys. Chem.* **2000**, *104*, 2120–2131.
(34) Noszal, B.; Rabenstein, D. L. Nitrogen-protonation microequilibria and C(2)-deprotonation microkinetics of histidine, histamine, and related compounds. *J. Phys. Chem.* **1991**, *95*, 4761–4765.
(35) Ganellin, C. R. The tautomer ratio of histamine. *J. Pharm. Pharmacol.* **1973**, *25*, 787–792.
(36) Jojart, B.; Martinek, T. A. Performance of the general amber force field in modeling aqueous POPC membrane bilayers. *J. Comput. Chem.* **2007**, *28*, 2051–2058.
(37) Phillips, J. C.; Braun, R.; Wang, W.; Gumbart, J.; Tajkhorshid, E.; Villa, E.; Chipot, C.; Skeel, R. D.; Kale, L.; Schulten, K. Scalable molecular dynamics with NAMD. *J. Comput. Chem.* **2005**, *26*, 1781–1802.
(38) Li, H.; Robertson, A. D.; Jensen, J. H. Very fast empirical prediction and rationalization of protein pKa values. *Proteins* **2005**, *61*, 704–721.
(39) Dolinsky, T. J.; Nielsen, J. E.; McCammon, J. A.; Baker, N. A. PDB2PQR: an automated pipeline for the setup of Poisson-Boltzmann electrostatics calculations. *Nucleic Acids Res.* **2004**, *32*, W665–W667.
(40) Bayly, C. I.; Cieplak, P.; Cornell, W. D.; Kollman, P. A. A well behaved electrostatic potential based method using charge restraints for deriving atomic charges: the RESP model. *J. Phys. Chem.* **1993**, *102*, 3787–3793.
(41) Molecular Operating Environment (MOE), 2005. 06; Chemical Computing Group, Inc.: 1255 University St. Suite 1600, Montreal, Quebec, Canada, 2005.
(42) Frisch, M. J.; Trucks, G. W.; Schlegel, H. B.; Scuseria, G. E.; Robb, M. A.; Cheeseman, J. R.; Montgomery, J. A., Jr.; Vreven, T.; Kudin, K. N.; Burant, J. C.; Millam, J. M.; Iyengar, S. S.; Tomasi, J.; Barone, V.; Mennucci, B.; Cossi, M.; Scalmani, G.; Rega, N.; Petersson, G. A.; Nakatsuji, H.; Hada, M.; Ehara, M.; Toyota, K.; Fukuda, R.; Hasegawa, J.; Ishida, M.; Nakajima, T.; Honda, Y.; Kitao, O.; Nakai, H.; Klene, M.; Li, X.; Knox, J. E.; Hratchian, H. P.; Cross, J. B.; Bakken, V.; Adamo, C.; Jaramillo, J.; Gomperts, R.; Stratmann, R. E.; Yazyev, O.; Austin, A. J.; Cammi, R.; Pomelli, C.; Ochterski, J. W.; Ayala, P. Y.; Morokuma, K.; Voth, G. A.; Salvador, P.; Dannenberg, J. J.; Zakrzewski, V. G.; Dapprich, S.; Daniels, A. D.; Strain, M. C.; Farkas, O.; Malick, D. K.; Rabuck, A. D.; Raghavachari, K.; Foresman, J. B.; Ortiz, J. V.; Cui, Q.; Baboul, A. G.; Clifford, S.; Cioslowski, J.; Stefanov, B. B.; Liu, G.; Liashenko, A.; Piskorz, P.; Komaromi, I.; Martin, R. L.; Fox, D. J.; Keith, T.; Al-Laham, M. A.; Peng, C. Y.; Nanayakkara, A.; Challacombe, M.; Gill, P. M. W.; Johnson, B.; Chen, W.; Wong, M. W.; Gonzalez, C.; Pople, J. A. *Gaussian 03*; Gaussian, Inc.: Wallingford, CT, 2004.
(43) Case, D. A.; Darden, T. A.; Cheatham, I. T. E.; Simmerling, C. L.; Wang, J.; Duke, R. E.; Luo, R.; Merz, K. M.; Wang, B.; Pearlman, D. A.; Crowley, M.; Brozell, S.; Tsui, V.; Gohlke, H.; Mongan, J.; Hornak, V.; Cui, G.; Beroza, P.; Schafmeister, C.; Caldwell, J. W.; Ross, W. S.; Kollman, P. A. *AMBER 8*; University of California: San Francisco, CA, 2004.
(44) Duan, Y.; Wu, C.; Chowdhury, S.; Lee, M. C.; Xiong, G.; Zhang, W.; Yang, R.; Cieplak, P.; Luo, R.; Lee, T.; Caldwell, J.; Wang, J.; Kollman, P. A point-charge force field for molecular mechanics simulations of proteins based on condensed-phase quantum mechanical calculations. *J. Comput. Chem.* **2003**, *24*, 1999–2012.
(45) Wang, J.; Wolf, R. M.; Caldwell, J. W.; Kollman, P. A.; Case, D. A. Development and testing of a general amber force field. *J. Comput. Chem.* **2004**, *25*, 1157–1174.
(46) Wang, J.; Wang, W.; Kollman, P. A.; Case, D. A. Automatic atom type and bond type perception in molecular mechanical calculations. *J. Mol. Graph. Model.* **2006**, *25*, 247–260.
(47) Darden, T.; York, D.; Pedersen, L. Particle mesh Ewald: an $N \cdot \log(N)$ method for Ewald sums in large systems. *J. Chem. Phys.* **1993**, *98*, 10089–10092.
(48) Case, D. A.; Darden, T. A.; Cheatham, I. T. E.; Simmerling, C. L.; Wang, J.; Duke, R. E.; Luo, R.; Merz, K. M.; Pearlman, D. A.; Crowley, M.; Walker, R. C.; Zhang, W.; Wang, B.; Hayik, S.; Roitberg, A.; Seabra, G.; Wong, K. F.; Paesani, F.; Wu, X.; Brozell, S.; Tsui, V.; Gohlke, H.; Yang, L.; Tan, C.; Mongan, J.; Hornak, V.; Cui, G.; Beroza, P.; Mathews, D. H.; Schafmeister, C.; Ross, W. S.; Kollman, P. A. *AMBER 9*; University of California: San Francisco, CA, 2006.
(49) Humphrey, W.; Dalke, A.; Schulten, K. VMD: visual molecular dynamics. *J. Mol. Graph.* **1996**, *14*, 33–38.
(50) Ratnala, V. R.; Kiihne, S. R.; Buda, F.; Leurs, R.; de Groot, H. J.; DeGrip, W. J. Solid-state NMR evidence for a protonation switch in the binding pocket of the H1 receptor upon binding of the agonist histamine. *J. Am. Chem. Soc.* **2007**, *129*, 867–872.
(51) Schoenlein, R. W.; Peteanu, L. A.; Mathies, R. A.; Shank, C. V. The first step in vision: femtosecond isomerization of rhodopsin. *Science* **1991**, *254*, 412–415.
(52) Ridge, K. D.; Palczewski, K. Visual rhodopsin sees the light: structure and mechanism of G protein signaling. *J. Biol. Chem.* **2007**, *282*, 9297–9301.
(53) Saam, J.; Tajkhorshid, E.; Hayashi, S.; Schulten, K. Molecular dynamics investigation of primary photoinduced events in the activation of rhodopsin. *Biophys. J.* **2002**, *83*, 3097–3112.
(54) Kong, Y.; Karplus, M. The signaling pathway of rhodopsin. *Structure* **2007**, *15*, 611–623.
(55) Springael, J. Y.; de Poorter, C.; Deupi, X.; Van Durme, J.; Pardo, L.; Parmentier, M. The activation mechanism of chemokine receptor CCR5 involves common structural changes but a different network of interhelical interactions relative to rhodopsin. *Cell. Signal.* **2007**, *19*, 1446–1456.
(56) Nakamichi, H.; Okada, T. Local peptide movement in the photoreaction intermediate of rhodopsin. *Proc. Natl. Acad. Sci. U.S.A.* **2006**, *103*, 12729–12734.
(57) Borhan, B.; Souto, M. L.; Imai, H.; Shichida, Y.; Nakanishi, K. Movement of retinal along the visual transduction path. *Science* **2000**, *288*, 2209–2212.
(58) Guo, W.; Shi, L.; Filizola, M.; Weinstein, H.; Javitch, J. A. Crosstalk in G protein-coupled receptors: changes at the transmembrane homodimer interface determine activation. *Proc. Natl. Acad. Sci. U.S.A.* **2005**, *102*, 17495–17500.
(59) Salom, D.; Lodowski, D. T.; Stenkamp, R. E.; Le Trong, I.; Golczak, M.; Jastrzebska, B.; Harris, T.; Ballesteros, J. A.; Palczewski, K. Crystal structure of a photoactivated deprotonated intermediate of rhodopsin. *Proc. Natl. Acad. Sci. U.S.A.* **2006**, *103*, 16123–16128.

CI700450W